PPARγ ablation sensitizes proopiomelanocortin neurons to leptin during high-fat feeding

Lihong Long,[1,2,3] Chitoku Toda,[1,2] Jing Kwon Jeong,[1,2] Tamas L. Horvath,[1,4,5] and Sabrina Diano[1,2,4,5]

[1]Program in Integrative Cell Signaling and Neurobiology of Metabolism and [2]Department of Obstetrics, Gynecology, and Reproductive Sciences, Yale University School of Medicine, New Haven, Connecticut, USA. [3]Department of Pharmacology, Tongji Medical College, Huazhong University of Science and Technology, Wuhan, China. [4]Department of Neurobiology and [5]Comparative Medicine, Yale University School of Medicine, New Haven, Connecticut, USA.

Activation of central PPARγ promotes food intake and body weight gain; however, the identity of the neurons that express PPARγ and mediate the effect of this nuclear receptor on energy homeostasis is unknown. Here, we determined that selective ablation of PPARγ in murine proopiomelanocortin (POMC) neurons decreases peroxisome density, elevates reactive oxygen species, and induces leptin sensitivity in these neurons. Furthermore, ablation of PPARγ in POMC neurons preserved the interaction between mitochondria and the endoplasmic reticulum, which is dysregulated by HFD. Compared with control animals, mice lacking PPARγ in POMC neurons had increased energy expenditure and locomotor activity; reduced body weight, fat mass, and food intake; and improved glucose metabolism when exposed to high-fat diet (HFD). Finally, peripheral administration of either a PPARγ activator or inhibitor failed to affect food intake of mice with POMC-specific PPARγ ablation. Taken together, our data indicate that PPARγ mediates cellular, biological, and functional adaptations of POMC neurons to HFD, thereby regulating whole-body energy balance.

Introduction

Pharmacological compounds that activate PPARs, such as thiazolidinediones, have been used as highly effective oral medications for type 2 diabetes due to their ability to increase systemic insulin sensitivity. An adverse effect of these compounds is weight gain (1, 2), which limits their potential applications for a variety of obesity-related metabolic diseases. Whether tissue-specific action of PPARs can explain this phenomenology is not known.

Several studies, including our own, have suggested a central role for PPARγ in whole-body energy homeostasis (3–7). Hypothalamic *Pparg* mRNA expression is several folds higher compared with *Ppara* or *Ppard* mRNA expression, and *Pparg* mRNA expression increases significantly in diet-induced obese (DIO) mice when compared with that of lean controls (7). While brain-specific deletion of PPARγ decreased food intake and increased energy expenditure (EE) in DIO mice (6), chronic hypothalamic-specific PPARγ activation induced increased food intake and body weight in DIO mice (5). In addition, deletion of PPARγ in the brain or in the hypothalamus conferred resistance to rosiglitazone-induced food intake and body weight gain (5, 6). Nevertheless, the identity of PPARγ-expressing neurons and the mode of action on cellular mechanisms in these cells that mediate the effect of PPAR agonists on energy homeostasis remains elusive.

We have shown that systemic administration of the PPARγ agonist, rosiglitazone, induced increased food intake on high-fat diet (HFD), a process that was associated with peroxisome proliferation, reduced reactive oxygen species (ROS) levels, and decreased activity of proopiomelanocortin (POMC) neurons in the arcuate nucleus of the hypothalamus (7). Whether PPARγ action within POMC neurons brings about these apparent crucial cellular biological adaptations in response to HFD is not known. To address this, we studied animals with POMC-specific deletion of PPARγ. We focused on cellular biological events and whole-body physiology of these animals and their control littermates.

Results

Generation and validation of Pomc-Cre Pparg$^{fl/fl}$ mice. To develop mice with selective ablation of PPARγ in POMC neurons, *Cre* transgenic mice, in which Cre recombinase is expressed specifically under the POMC promoter were crossed with *Pparg$^{fl/fl}$* mice (Jackson Lab). In situ hybridization for *Pparg* mRNA combined with POMC immunocytochemistry showed colocalization in control mice (Supplemental Figure 1; supplemental material available online with this article; doi:10.1172/JCI76220DS1), while no colocalization was observed in *Pomc-Cre Pparg$^{fl/fl}$* mice (Supplemental Figure 1), confirming PPARγ deletion in the hypothalamic POMC neurons. Because POMC promoter also drives Cre recombinase expression in the pituitary, we examined the pituitary-adrenal axis. The expression levels of *Pomc* mRNA (1.00 ± 0.11 in male controls vs. 1.04 ± 0.12 in male *Pomc-Cre Pparg$^{fl/fl}$* mice) as well as circulating corticosterone levels (46.6 ± 9.9 ng/ml in male controls vs. 47.1 ± 10.8 ng/ml in male *Pomc-Cre Pparg$^{fl/fl}$* mice) were unaltered between the 2 genotypes. These data suggest that deletion of PPARγ in the pituitary does not affect the pituitary-adrenal axis.

Deletion of PPARγ in POMC neurons does not alter energy balance on standard chow diet. On a standard chow diet, no difference in body weight was found among female (Supplemental Figure 2A) and male (Supplemental Figure 3A) *Pomc-Cre Pparg$^{fl/fl}$*, *Pomc-Cre Pparg$^{fl/+}$*, and *Pparg$^{fl/fl}$* (Cre negative defined as control)

Conflict of interest: The authors have declared that no conflict of interest exists.
Submitted: March 19, 2014; **Accepted:** June 12, 2014.
Reference information: *J Clin Invest*. 2014;124(9):4017–4027. doi:10.1172/JCI76220.

mice up to 16 weeks of age. The amount of adipose depot in both female (Supplemental Figure 2, B and C) and male (Supplemental Figure 3, B and C) *Pomc-Cre Pparg*$^{fl/fl}$ mice was not statistically significant compared with that of *Pomc-Cre Pparg*$^{fl/+}$ and control mice. Leptin levels were also similar between *Pomc-Cre Pparg*$^{fl/fl}$ and control groups (1.15 ± 0.09 ng/ml in female *Pomc-Cre Pparg*$^{fl/fl}$ mice vs. 1.38 ± 0.05 ng/ml in controls; $P > 0.05$). EE and locomotor activity in both females and males were also similar between *Pomc-Cre Pparg*$^{fl/fl}$ and control mice (Supplemental Figure 2 and Supplemental Figure 3, D–H). No differences in thyroid hormones levels were found between these experimental groups (data not shown). When food intake was measured in a 24-hour period, female and male *Pomc-Cre Pparg*$^{fl/fl}$ mice showed no significant difference in feeding compared to that of control mice (females: 3.61 ± 0.16 g in *Pomc-Cre Pparg*$^{fl/fl}$ mice vs. 3.78 ± 0.15 g in controls; males: 3.86 ± 0.06 g in *Pomc-Cre Pparg*$^{fl/fl}$ mice vs. 4.02 ± 0.31 g in controls).

Loss of PPARγ in POMC neurons decreases peroxisome density and increases ROS levels in POMC neurons of HFD-exposed mice. Exposure to HFD significantly increases peroxisome density and decreases ROS levels in POMC neurons (7). To test the involvement of PPARγ, we analyzed peroxisome density and ROS levels in HFD-exposed *Pomc-Cre Pparg*$^{fl/fl}$ and control mice. A significant reduction in peroxisome density was observed in POMC neurons of *Pomc-Cre Pparg*$^{fl/fl}$ mice compared with in control mice (0.31 ± 0.05 peroxisomes/μm^2 POMC cytosols in *Pomc-Cre Pparg*$^{fl/fl}$ mice vs. 0.58 ± 0.07 peroxisomes/μm^2 POMC cytosols in control littermates, $P < 0.05$; Figure 1, A and B). POMC neurons of *Pomc-Cre Pparg*$^{fl/fl}$ mice also showed significantly greater ROS levels (6.26 ± 0.37 fluorescent particles in 10 μm^2 cytosol) than those of control mice (4.23 ± 0.38 fluorescent particles in 10 μm^2 cytosol; $P < 0.05$; Figure 1, C and D).

Loss of PPARγ in POMC neurons induces increased POMC neuronal activity of HFD-exposed mice. Increased ROS levels in POMC neurons have been associated with increased POMC neuronal activity (7, 8). In agreement with these studies, a greater percentage of POMC neurons in *Pomc-Cre Pparg*$^{fl/fl}$ mice (19.20% ± 2.60%) showed c-fos staining in their nuclei compared with control mice (9.30% ± 1.81%; Figure 1, E and F).

Ablation of PPARγ in POMC neurons prevents hyperphagia and alters energy balance on HFD. The body weight of both female and male *Pomc-Cre Pparg* mice on HFD for 16 weeks was significantly lower than that of control mice. In female mice, a significant difference in body weight appeared as soon as 2 weeks of HFD feeding (Figure 2A). Female *Pomc-Cre Pparg* mice showed resistance to high-fat feeding, reaching an average body weight of 23.49 ± 0.99 g compared with that of control mice after 16 weeks of HFD exposure 27.44 ± 1.42 g ($P = 0.03$) (Figure 2A). On the other hand, the difference in body weight between males became evident later, at 9 weeks of HFD feeding (32.47 ± 0.48 g in controls and 30.22 ± 0.59 g in *Pomc-Cre Pparg*$^{fl/fl}$ mice), and after 16 weeks of HFD feeding, the average body weight of male *Pomc-Cre Pparg*$^{fl/fl}$ mice was 33.60 ± 1.98 g, while that for control mice was 39.62 ± 1.55 g ($P < 0.05$) (Figure 2B). *Pomc-Cre Pparg*$^{fl/fl}$ mice were also significantly lighter than *Pomc-Cre Pparg*$^{fl/+}$ mice (Supplemental Figure 4) at 9 weeks of HFD, indicating that the effect on body weight between the controls (*Pparg*$^{fl/fl}$*-Cre* negative) and the *Pomc-Cre Pparg*$^{fl/fl}$ mice was not due to the presence of the *Pomc-Cre* transgene. Consistent with the body weights, significant changes in body composition were observed (Figure 2, C–F). A decrease in fat mass (Figure 2, C and D) was observed in both female and male *Pomc-Cre Pparg*$^{fl/fl}$ mice compared with control littermates. The significant difference in fat mass in both males and females was reached at around 4 weeks of HFD exposure and persisted for the duration of the experiment (female fat mass at 16 weeks of HFD: 3.67 ± 0.37 g in *Pomc-Cre Pparg*$^{fl/fl}$ mice vs. 8.14 ± 1.45 g in control mice, Figure 2C; male fat mass at 16 weeks of HFD: 8.59± 1.25 g in *Pomc-Cre Pparg*$^{fl/fl}$ mice vs. 13.44± 1.13 g in control mice, $P < 0.05$, Figure 2D). Consistently, leptin levels were significantly ($P = 0.009$) lower in *Pomc-Cre Pparg*$^{fl/fl}$ mice (13.9 ± 1.6 ng/ml) compared with those in littermate controls (21.7 ± 1.2 ng/ml). No difference in lean mass was observed between groups (Figure 2, E and F).

To understand the cause of reduced body weight gain, we then measured food intake. Twenty-four–hour food intake analysis showed a slight but not significant decrease in food consumption in *Pomc-Cre Pparg*$^{fl/fl}$ animals compared with that in the controls on HFD (2.75 ± 0.21 g in female controls vs. 2.38 ± 0.15 g female *Pomc-Cre Pparg*$^{fl/fl}$ mice, $P > 0.05$, $n = 5$, Figure 3A; 2.87 ± 0.18 g in male controls vs. 2.68 ± 0.17 g in male *Pomc-Cre Pparg*$^{fl/fl}$ mice, $P > 0.05$, Figure 3B). However, when food intake was analyzed during the dark-and-light cycles, a significant difference in food intake was found during the dark phase (1.48 ± 0.17 g in female controls vs. 1.13 ± 0.09 g in female *Pomc-Cre Pparg*$^{fl/fl}$ mice, $P < 0.05$, Figure 3A; 1.40 ± 0.13 g in male *Pomc-Cre Pparg*$^{fl/fl}$ mice vs. 2.03 ± 0.22 g in male controls, $P < 0.05$, Figure 3B). No difference was observed during the light phase in both female mice (Figure 3A) and male mice (Figure 3B).

We then measured EE and locomotor activity in male and female *Pomc-Cre Pparg*$^{fl/fl}$ mice and controls on HFD. Male *Pomc-Cre Pparg*$^{fl/fl}$ mice showed no difference in EE compared with that of controls when EE was normalized by lean mass (Figure 4A). However, when EE was analyzed using analysis of covariance (ANCOVA), a significant increase was observed in male *Pomc-Cre Pparg*$^{fl/fl}$ mice compared with that in controls (Figure 4B; 12.259 ± 0.136 kcal per day in *Pomc-Cre Pparg*$^{fl/fl}$ mice vs. 11.374 ± 0.123 kcal per day in controls, $P < 0.05$ both for body weight and genotype effects). Furthermore, EE was significantly increased during the light cycle (11.754 ± 0.211 kcal per day in *Pomc-Cre Pparg*$^{fl/fl}$ mice and 10.738 ± 0.190 kcal per day in controls, $P < 0.05$ both for body weight and genotype effects), but not during the dark cycle (12.482 ± 0.338 kcal per day in *Pomc-Cre Pparg*$^{fl/fl}$ mice and 12.023 ± 0.304 kcal per day in controls; $P < 0.05$ for body weight effect; $P = 0.38$ for genotype effect). Elevated levels of VO_2 (2,369.675 ± 24.604 ml per day in controls and 2,545.735 ± 27.360 ml per day in *Pomc-Cre Pparg*$^{fl/fl}$ mice, $P < 0.05$ both for body weight and genotype effects, Figure 4C) and VCO_2 (1,839.580 ± 29.576 ml per day in controls and 2,014.103 ± 32.888 ml per day in *Pomc-Cre Pparg*$^{fl/fl}$ mice, $P < 0.05$ both for body weight and genotype effects; Figure 4D) were also observed in *Pomc-Cre Pparg*$^{fl/fl}$ mice compared with control mice. No difference in the respiratory exchange rate (0.778 ± 0.010 in controls and 0.785 ± 0.013 in *Pomc-Cre Pparg*$^{fl/fl}$ mice) was observed (Figure 4E).

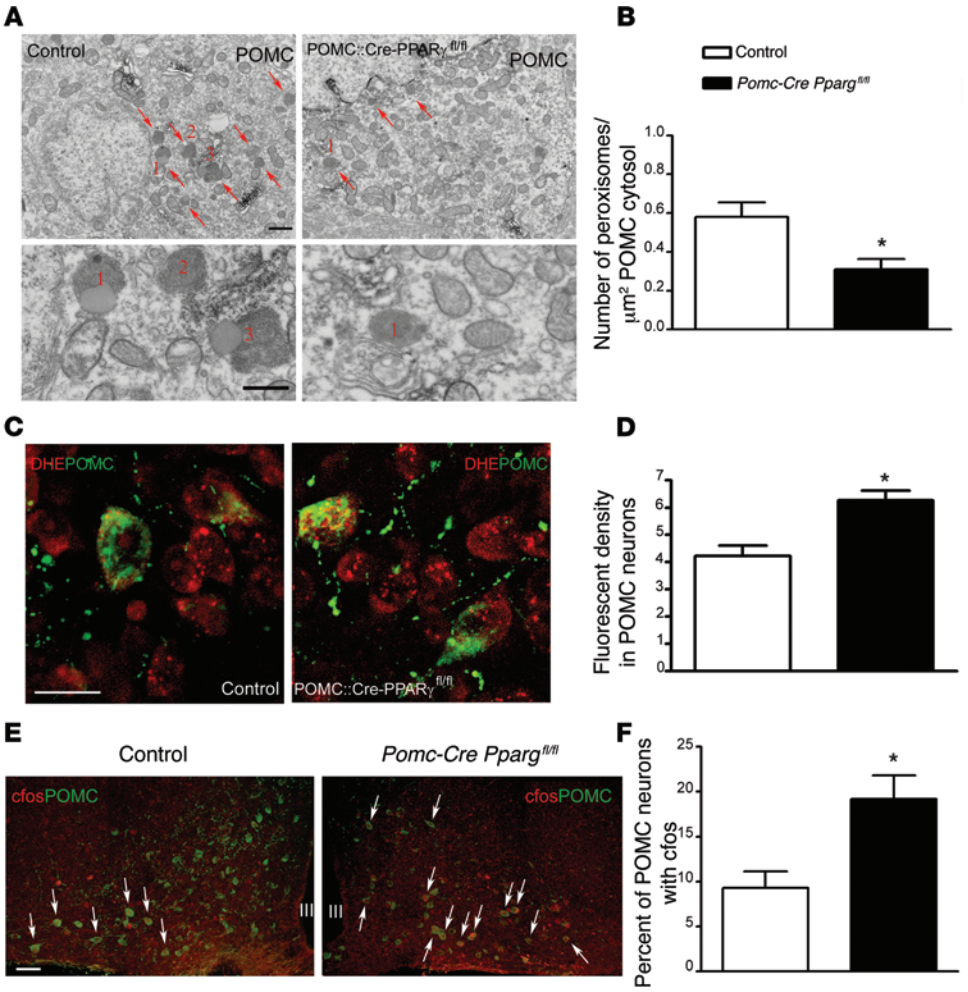

Figure 1. Lower peroxisome density and elevated ROS levels and neuronal activation in POMC neurons of *Pomc-Cre Pparg*$^{fl/fl}$ mice on HFD. (**A**) Electron micrographs showing representative sections of POMC perikarya in the arcuate nuclei of control and *Pomc-Cre Pparg*$^{fl/fl}$ mice. Red arrows point to peroxisomes. Images on bottom row are high-power magnification images of peroxisomes from the top row, respectively (numbers in images on the top row correspond with numbers in images on the bottom row). Scale bars: 500 nm. (**B**) Graph showing significantly lower peroxisome density in *Pomc-Cre Pparg*$^{fl/fl}$ animals compared with controls (n = 4 per group). (**C**) Representative confocal micrographs from control and *Pomc-Cre Pparg*$^{fl/fl}$ mice fed on HFD showing DHE (red) in POMC neurons (green). Scale bar: 20 μm. (**D**) Graph showing the density levels of DHE in POMC neurons of control (n = 4) and *Pomc-Cre Pparg*$^{fl/fl}$ mice (n = 4). (**E**) Representative confocal micrographs of double labeling for c-fos (red nuclei) and POMC (green cytoplasm) showing colocalization (white arrows) in the arcuate nucleus of the hypothalamus of a control and a *Pomc-Cre Pparg*$^{fl/fl}$ mouse fed on HFD. Scale bar: 50 μm. III, third ventricle. (**F**) Graph showing a significant increase in the percentage of c-fos/POMC double-labeled neurons in *Pomc-Cre Pparg*$^{fl/fl}$ mice compared with control littermates on HFD (n = 4 per group). Data in all graphs are shown as mean ± SEM. *P < 0.05.

The total locomotor activity of *Pomc-Cre Pparg*$^{fl/fl}$ mice on HFD was significantly higher than that of controls (56,217 ± 2,902 beam breaks per 48 hours in controls and 63,796 ± 3,680 beam breaks per 48 hours in *Pomc-Cre Pparg*$^{fl/fl}$ mice, P < 0.05; Figure 4F). This difference was due to an increased locomotor activity during both dark (41,379 ± 3,052 beam breaks per 48 hours in controls and 45,348 ± 2,342 beam breaks per 48 hours in *Pomc-Cre Pparg*$^{fl/fl}$ mice, P < 0.05; Figure 4F) and light phases (14,837 ± 1,140 beam breaks per 48 hours in controls and 18,448 ± 1,890 beam breaks per 48 hours in *Pomc-Cre Pparg*$^{fl/fl}$ mice, P < 0.05; Figure 4F).

To further analyze the increase in EE, we then assessed the expression of uncoupling protein 1 (UCP1) in the brown adipose tissues (BATs). A significant increase in *Ucp1* mRNA was observed in *Pomc-Cre Pparg*$^{fl/fl}$ mice compared with their littermate controls (Figure 4G). However, no differences in thyroid hormone levels were observed between the 2 groups (free T3: 3.1 ± 0.8 ng/dl, n = 4 male controls vs. 3.6 ± 1.9 ng/dl, n = 6 male *Pomc-Cre Pparg*$^{fl/fl}$ mice; free T4: 1.9 ± 0.7 ng/dl, n = 4 male controls vs. 1.4 ± 0.3 ng/dl, n = 5 male *Pomc-Cre Pparg*$^{fl/fl}$ mice).

Female *Pomc-Cre Pparg*$^{fl/fl}$ mice showed increased EE compared with control mice on HFD both after normalization to lean mass (Supplemental Figure 5A) or after ANCOVA analysis (Supplemental Figure 5B; 11.279 ± 0.206 kcal per day in *Pomc-Cre Pparg*$^{fl/fl}$ mice vs. 10.594 ± 0.186 kcal per day in controls, P < 0.05 both for body weight and genotype effects). In contrast to the males, EE was significantly greater during the dark cycle in females (12.078 ± 0.202 kcal per day in *Pomc-Cre Pparg*$^{fl/fl}$ mice and 11.259 ± 0.0.183 kcal per day in controls, P < 0.05 for body weight and genotype effects) but not during the light cycle (10.499 ± 0.244 kcal per day in *Pomc-Cre Pparg*$^{fl/fl}$ mice and 9.946 ± 0.221 kcal per day in controls, P < 0.05 both for body weight effect; P = 0.149 for genotype effect). Elevated levels of VO_2 (2,199.616 ± 37.778 ml per day in controls and 2,338.401 ± 41.809 ml per day in *Pomc-Cre Pparg*$^{fl/fl}$ mice, P < 0.05 both for body weight and genotype effects; Supplemental Figure 5C) and VCO_2 (1,741.982 ± 34.032 ml per day in controls and 1,864.273 ± 37.663 ml per day in *Pomc-Cre Pparg*$^{fl/fl}$ mice, P < 0.05 for body weight effects, P = 0.052 for genotype effect; Supplemental Figure 5D) were also observed in *Pomc-Cre Pparg*$^{fl/fl}$ mice compared with control mice. No difference in the respiratory exchange rate (0.792 ± 0.005 in controls and 0.793 ± 0.004 in *Pomc-Cre Pparg*$^{fl/fl}$ mice, Supplemental Figure 5E) was observed. The total locomotor activity of *Pomc-Cre Pparg*$^{fl/fl}$ mice on HFD was significantly higher than that of controls (104,898 ± 8,851 beam breaks per 48 hours in controls and 157,906 ± 30,918 beam breaks per 48 hours in *Pomc-Cre Pparg*$^{fl/fl}$ mice, P < 0.05, Supplemental Figure

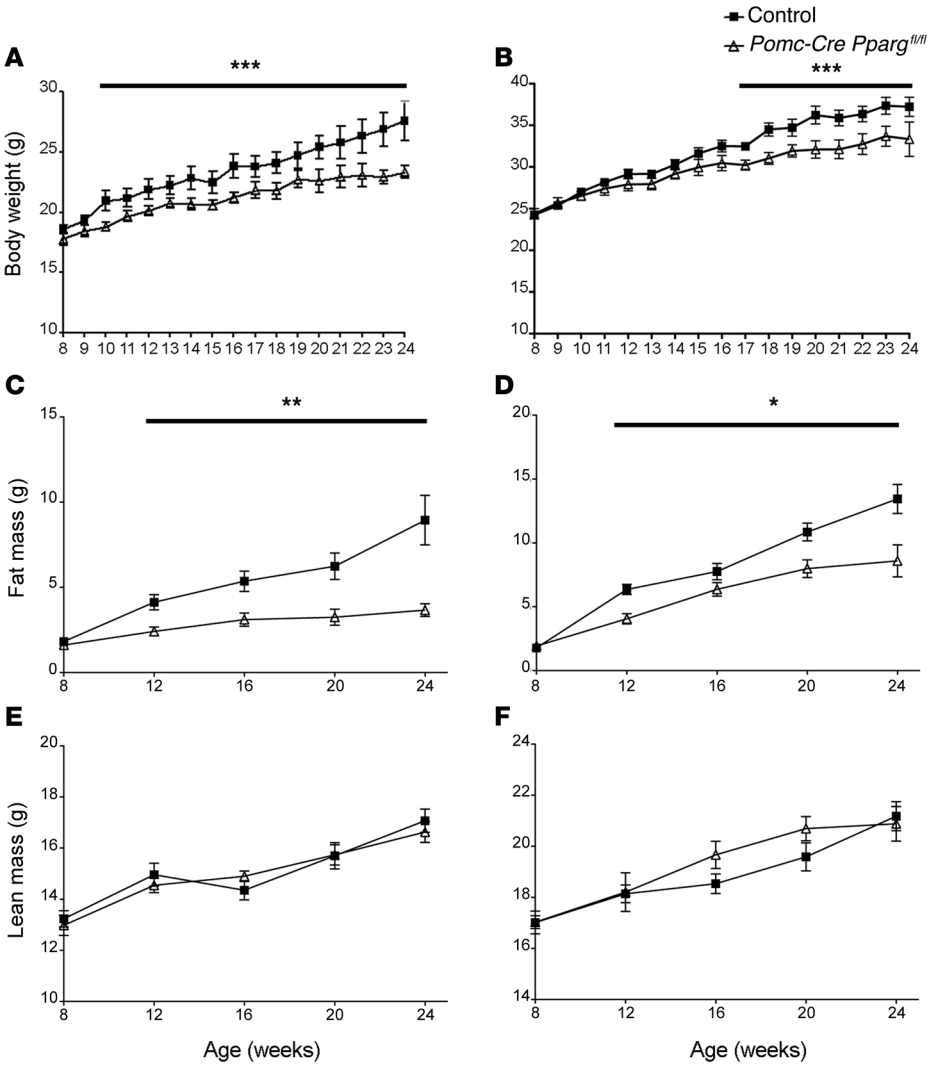

Figure 2. Lower peroxisome density and elevated ROS levels and neuronal activation in POMC neurons of *Pomc-Cre Pparg*$^{fl/fl}$ mice on HFD is associated with a leaner phenotype. Analysis of (**A** and **B**) body weight (n = 9–14 per group), (**C** and **D**) fat mass (n = 9–14 per group), and (**E** and **F**) lean mass (n = 9–14 per group) showed that both (**A**, **C**, and **E**) female and (**B**, **D**, and **F**) male *Pomc-Cre Pparg*$^{fl/fl}$ mice were resistant to HFD compared with littermate controls. Data in all graphs are shown as mean ± SEM. $^*P < 0.05$; $^{**}P < 0.01$; $^{***}P < 0.001$.

5F). This difference was due to an increased locomotor activity during both the dark phase (77,675 ± 5,783 beam breaks per 48 hours in controls and 102,227 ± 6031 beam breaks per 48 hours in *Pomc-Cre Pparg*$^{fl/fl}$ mice, $P < 0.05$, Supplemental Figure 5F) and the light phase (23,527 ± 1,271 beam breaks per 48 hours in controls and 35,361 ± 2,622 beam breaks per 48 hours in *Pomc-Cre Pparg*$^{fl/fl}$ mice, $P < 0.05$, Supplemental Figure 5F).

Insulin sensitivity in Pomc-Cre Pparg$^{fl/fl}$ *mice*. Analysis of glucose and insulin tolerance tests showed a greater glucose tolerance and insulin sensitivity of *Pomc-Cre Pparg*$^{fl/fl}$ mice compared with control littermates (Figure 5, A and B). No difference in insulin levels was found between the 2 experimental groups in fasted (0.31 ± 0.07 ng/ml in female *Pomc-Cre Pparg*$^{fl/fl}$ mice vs. 0.31 ± 0.02 ng/ml in control mice) or fed conditions (2.30 ± 0.57 ng/ml in female *Pomc-Cre Pparg*$^{fl/fl}$ mice vs. 2.19 ± 0.88 ng/ml in control mice). Liver analysis showed a decrease in the mRNA levels of hepatic gluconeogenesis enzymes, such as phosphoenolpyruvate carboxykinase (*Pepck*) (0.53 ± 0.06 in male *Pomc-Cre Pparg*$^{fl/fl}$ mice vs. 0.92 ± 0.15 in controls, $P < 0.05$, Figure 5C) and glucose-6-phosphatase (*G6pase*) (0.34 ± 0.07 in male *Pomc-Cre Pparg*$^{fl/fl}$ mice vs. 1.00 ± 0.25 in controls, $P < 0.05$, Figure 5D) in *Pomc-Cre Pparg*$^{fl/fl}$ mice compared with control littermates, indicating an increased hepatic insulin sensitivity in these mice.

To further analyze glucose metabolism in *Pomc-Cre Pparg*$^{fl/fl}$ mice, we performed hyperinsulinemic euglycemic clamp on mice on 9 weeks of HFD. To maintain blood glucose levels between 110 mg/dl and 130 mg/dl in both groups (Figure 6A), we needed to infuse approximately 2-fold glucose into *Pomc-Cre Pparg*$^{fl/fl}$ mice compared with control mice (the average glucose infusion rate between t = 75 minutes and t = 115 minutes was 8.6 ± 2.2 mg/kg/min in controls, n = 7, and 16.8 ± 2.8 mg/kg/min in *Pomc-Cre Pparg*$^{fl/fl}$ mice, n = 6, Figure 6B), suggesting that *Pomc-Cre Pparg*$^{fl/fl}$ mice had higher insulin sensitivity than control mice. Consistent with this, *Pomc-Cre Pparg*$^{fl/fl}$ mice had a significantly higher rate of disappearance (Rd), which represents whole-body glucose utilization during the clamp period, compared with control mice (16.6 ± 1.7 mg/kg/min in control mice and 21.6 ± 1.3 mg/kg/min in *Pomc-Cre Pparg*$^{fl/fl}$ mice, Figure 6C). Simultaneously, *Pomc-Cre Pparg*$^{fl/fl}$ mice also showed increased insulin-stimulated inhibition of endogenous glucose production, which mainly represents hepatic insulin sensitivity (40.2% ± 6.3% in controls and 68.2% ± 10.0% in *Pomc-Cre Pparg*$^{fl/fl}$ mice, Figure 6D). In agreement with the result of Rd, *Pomc-Cre Pparg*$^{fl/fl}$ mice had significantly greater 2-deoxy-D-glucose (2DG) uptake in epididymal white adipose tissue (EWAT) (Figure 6E; 3.4 ± 0.4 nmol/g/min in control mice and 5.9 ± 0.4 nmol/g/min in *Pomc-Cre Pparg*$^{fl/fl}$ mice), soleus, and the red portion of gastrocnemius muscle (Gastro-R) compared with that of control mice during the clamp period (soleus: 100.3 ± 18.4 nmol/g/min in controls and 188.5 ± 37.0 nmol/g/min in *Pomc-Cre Pparg*$^{fl/fl}$ mice; Gastro-R: 27.8 ± 4.0 nmol/g/min in controls and 58.6 ± 9.6 nmol/g/min in *Pomc-Cre Pparg*$^{fl/fl}$ mice; Figure 6F). 2DG uptake in both spleens and brains, which are not insulin-sensitive tissue, were not significantly different between groups (Figure 6G). These results suggest that deletion of PPARγ in POMC neurons improves glucose metabolism due to the enhancement of insulin sensitivity in EWAT, muscle, and liver during HFD feeding.

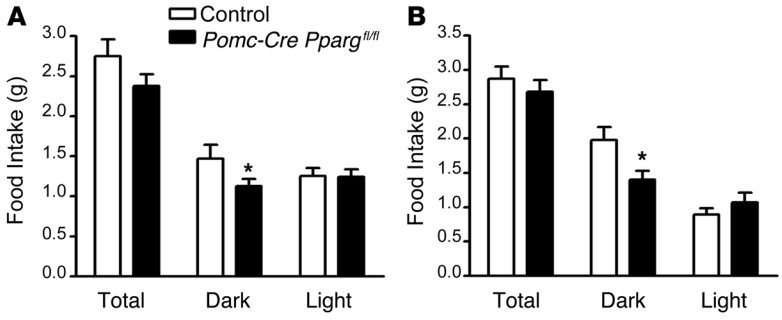

Figure 3. *Pomc-Cre Pparg*$^{fl/fl}$ mice on HFD have reduced feeding. Analysis of daily food intake in (**A**) female (n = 5–6 per group) and (**B**) male (n = 9–12 per group) mice on HFD shows that in both genders *Pomc-Cre Pparg*$^{fl/fl}$ mice ate less than control littermates. This difference in food intake was significant during the dark cycle in both female and male mice. Data in all graphs are shown as mean ± SEM. *P < 0.05 compared with controls.

PPARγ deletion in POMC neurons increases leptin sensitivity on HFD. To test leptin sensitivity, HFD-fed *Pomc-Cre Pparg*$^{fl/fl}$ and control mice were i.p. injected with leptin twice a day for 3 days, with a dose of leptin of 1.5 μg/g body weight. Compared with controls, *Pomc-Cre Pparg*$^{fl/fl}$ mice showed a significant reduction in food intake (day 3: –30% ± 6.59% reduction of food intake) compared with control littermates (day 3: –12.42% ± 2.65% reduction food intake, P < 0.05 vs. WT mice, Figure 7A). *Pomc-Cre Pparg*$^{fl/fl}$ mice also showed a significant reduction in body weight gain (day 3: 1.80% ± 0.72% in control vs. 5.41% ± 0.60% of *Pomc-Cre Pparg*$^{fl/fl}$ mice; P < 0.05 vs. control mice, Figure 7B).

To assess activation of the leptin-associated signal pathway, p-STAT3 immunoreactivity was analyzed after leptin treatment. After i.p. leptin injection, p-STAT3 expression in POMC neurons was significantly increased in *Pomc-Cre Pparg*$^{fl/fl}$ mice (45.63% ± 4.91%) compared with control mice on HFD (19.42% ± 4.04%, Figure 7, C and D). Similarly, c-fos immunostaining in POMC neurons was significantly higher in *Pomc-Cre Pparg*$^{fl/fl}$ mice (24.28% ± 3.90%) compared with that in control littermates (6.00% ± 2.09%, Figure 7, E and F).

Endoplasmic reticulum (ER) stress plays a key role in the development of obesity and leptin resistance (9, 10). Recently, close interaction between mitochondria and ER has been shown to play an important role in the onset of obesity and leptin resistance (11). Analysis of mitochondria-ER interaction in our study showed that the number of mitochondria-ER contacts in POMC neurons of *Pomc-Cre Pparg*$^{fl/fl}$ mice was significantly greater (53.05 ± 2.71) than those in POMC neurons of control mice (23.35 ± 3.61, P < 0.001, Figure 7, G and H)

PPARγ in POMC neurons mediates rosiglitazone and GW9662 effects on food intake. To assess whether the effects of PPARγ activation or inhibition are mediated by PPARγ expression in POMC neurons, we then assessed food intake of *Pomc-Cre Pparg*$^{fl/fl}$ and control mice treated i.p. with either rosiglitazone, a PPARγ agonist, or GW9662, a PPARγ antagonist, for 5 days.

Rosiglitazone administration to lean control mice exposed to HFD caused a significant increase in food intake (23.3% ± 3.03%) and body weight gain (4.47% ± 0.63%) compared with *Pomc-Cre Pparg*$^{fl/fl}$ mice (–0.2% ± 8.4% food intake and 1.08% ± 1.16% body weight, P < 0.05, Figure 8, A and B, respectively).

Similarly, GW9662 administration to HFD-exposed mice for 16 weeks significantly reduced food intake (–11.87% ± 3.86%) and body weight change (–4.95% ± 1.16%) in control mice compared with *Pomc-Cre Pparg*$^{fl/fl}$ mice (1.42% ± 4.22% food intake and –0.41% ± 0.28% body weight, P < 0.05, Figure 8, C and D, respectively).

Discussion

The results of this study unmasked a crucial role for PPARγ in POMC neurons to bring about cellular biological adaptations of these cells to the changing metabolic environment. We showed that the arcuate nucleus POMC neurons are important sites of action of PPARγ during high-fat feeding. We showed that deletion of PPARγ in POMC neurons attenuates hyperphagia, increases EE, and protects the mice from DIO and the development of leptin resistance. The cellular mechanisms responsible for these effects involve proliferation of peroxisomes, changes in ROS levels, and mitochondrial ER interactions. Ablation of PPARγ in POMC neurons prevented the increase of peroxisome density and increased ROS levels and mitochondrial ER in association with higher activity of POMC neurons. Considering that PPARγ is widely expressed within the central nervous system, our work also highlights PPARγ as a potential general metabolic switch of neurons.

Pomc-Cre Pparg$^{fl/fl}$ mice exposed to HFD showed a decrease in body weight gain compared with control littermates. The reduced body weight in *Pomc-Cre Pparg*$^{fl/fl}$ mice was due to a marked decrease in adipose mass, induced by a significant decrease in food intake and increase in EE, locomotor activity, and BAT activity in *Pomc-Cre Pparg*$^{fl/fl}$ mice. In agreement with these data, *Pomc-Cre Pparg*$^{fl/fl}$ mice showed an improved glucose metabolism compared with controls. Interestingly, a previous report using a mouse model in which PPARγ was deleted in the whole brain, BPPARγKO (synapsin I-Cre mice; ref. 6), showed that these mice, while having a reduced body weight gain when exposed to HFD, did not show improvements in their glucose metabolism (6). Our study shows that *Pomc-Cre Pparg*$^{fl/fl}$ mice have a significantly greater insulin sensitivity in several tissues, including muscle and white adipose tissue, compared with controls, which was associated with a downregulation of hepatic enzymes involved in the gluconeogenesis and an increased insulin-induced inhibition of endogenous glucose production in the liver. However, no difference in glucose tolerance or insulin-induced suppression of hepatic glucose production was found in BPPARγKO mice compared with controls, despite the differences in body weight and body composition (6). Thus, this observation suggests that the improved glucose tolerance and insulin sensitivity may be independent of changes in body weight and body composition.

By binding its receptors on cell membrane, leptin activates POMC neurons and exerts its anorexigenic effect and increases EE (12). Increased activity of POMC neurons has been associated with elevated intracellular ROS levels (7, 8). Thus, during DIO, sustained higher levels of leptin would predict higher intracellular levels of ROS and activity of POMC neurons. However, during DIO leptin resistance (13), a phenomenon characterized by the inability

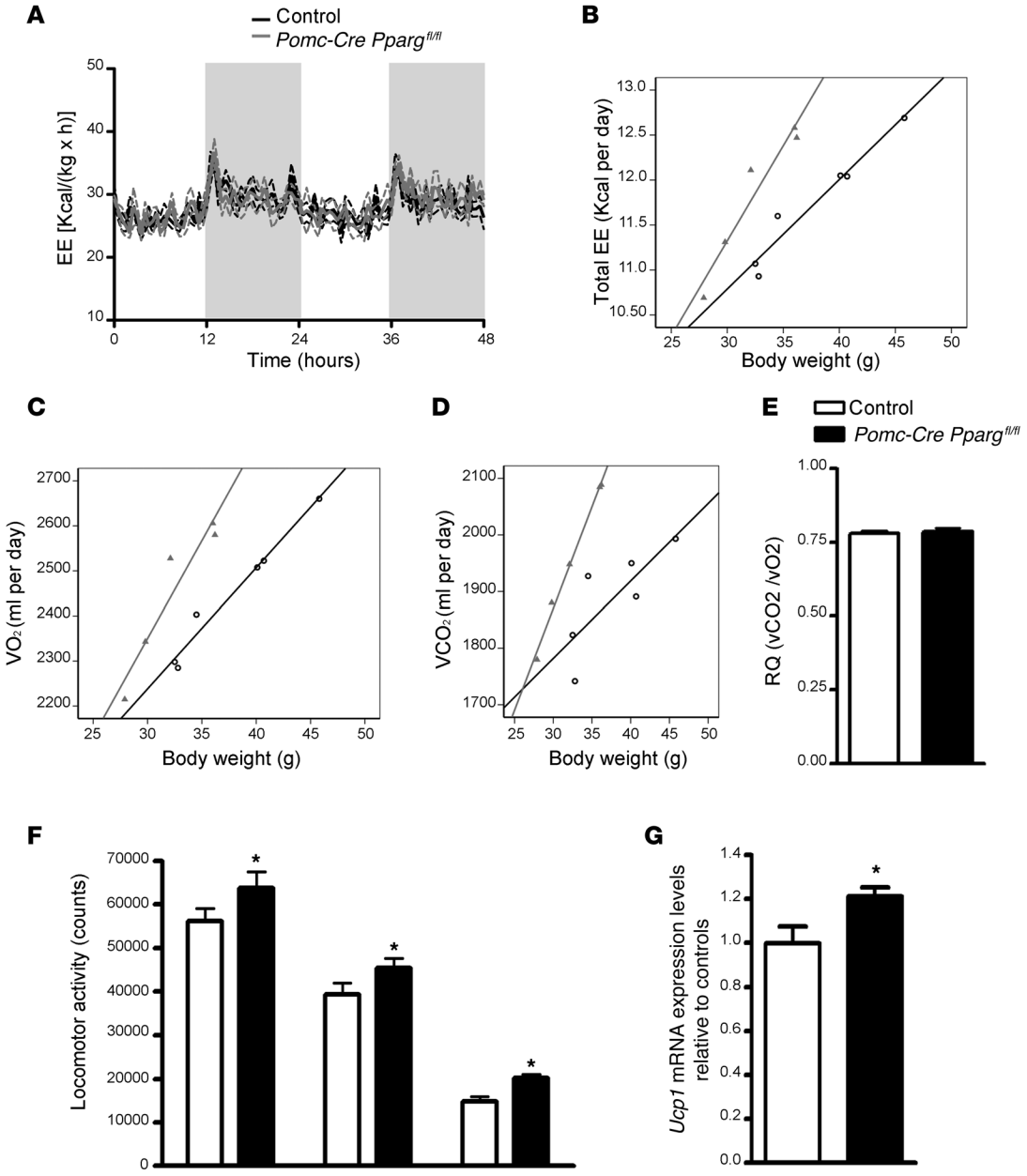

Figure 4. *Pomc-Cre Pparg*$^{fl/fl}$ mice on HFD have increased EE. (**A** and **B**) The results of EE analysis either after normalization by (**A**) lean mass or (**B**) ANCOVA analysis between male *Pomc-Cre Pparg*$^{fl/fl}$ and control mice (n = 5–6 per group). (**C** and **D**) The results of (**C**) VO_2 and (**D**) VCO_2 analysis in male *Pomc-Cre Pparg*$^{fl/fl}$ and control mice using ANCOVA (n = 5–6 per group). (**E**) No difference in respiratory quotient (RQ) was found between the 2 groups. (**F**) Increased locomotor activity during both dark and light cycles of male *Pomc-Cre Pparg*$^{fl/fl}$ mice compared with male controls. (**G**) Elevated BAT *Ucp1* mRNA expression levels in male *Pomc-Cre Pparg*$^{fl/fl}$ mice (n = 7) compared with male controls (n = 4). Data in all graphs are shown as mean ± SEM. *P < 0.05 compared with controls.

of exogenously administered leptin to induce Stat3 phosphorylation and simultaneously by an increase in suppressor of cytokine signaling 3 (SOC3) (14, 15), develops, and the positive correlation between circulating leptin levels and intracellular ROS levels in POMC cells is lost (7). Interestingly, an increase in peroxisome density in POMC neurons occurs in DIO mice (7). Peroxisomes are cellular organelles involved in the catabolism of long-chain fatty acids through β-oxidation (16, 17). Peroxisomes also contain several enzymes, including catalase, which, by using hydrogen peroxidase to oxidize several substrates, detoxify the cell from deleterious ROS (18). Thus, the increase of peroxisome density in POMC neurons of DIO mice, caused by decreasing ROS levels, may affect POMC activity and sensitivity to leptin. In support of this, our data show that preventing the increase of peroxisome density in POMC neurons by selective deletion of PPARγ induces an elevation in ROS levels together with increased POMC activity and leptin sensitivity.

Our study shows that mice with deletion of PPARγ in POMC neurons have a significant increase in mitochondria-ER interaction compared with controls. ER stress and mitochondrial dysfunction are implicated in the pathogenesis of obesity and leptin resistance (9–11, 19). Disruption of mitochondria-ER interaction was shown recently to be a key element in leptin resistance of POMC neurons specifically (11). Thus, our observation that PPARγ deletion in POMC neurons reversed the loss of mitochondria-ER connection in response to HFD highlights the importance of PPARγ in the etiology of ER stress.

Our study assessed the effect of constitutive loss of PPARγ during development in POMC neurons. Gene deletion during development may induce compensatory mechanisms that may affect the overall metabolic phenotype of an organism and undermine the significance of that gene in the regulation of homeostasis. This is the case for AgRP neuron deletion, which has been

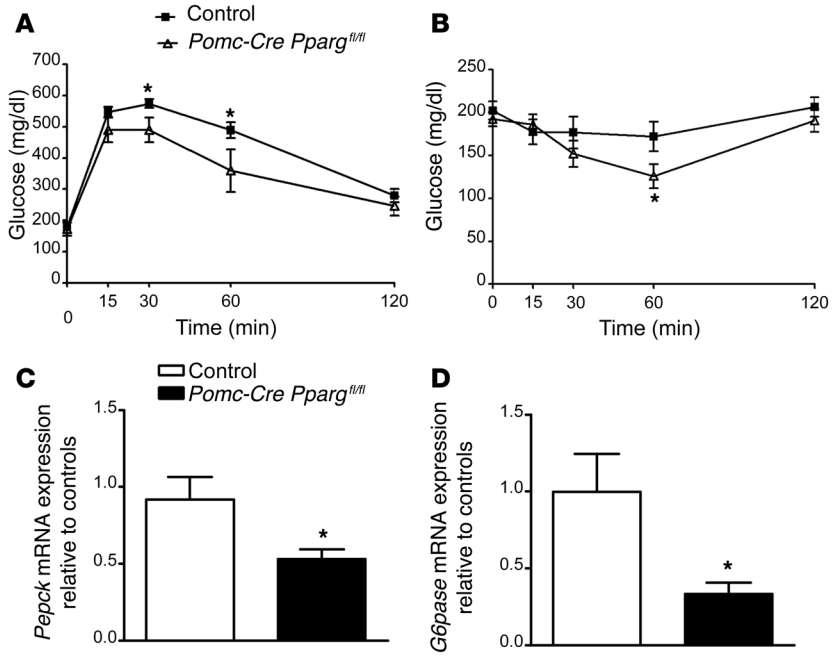

Figure 5. *Pomc-Cre Pparg*$^{fl/fl}$ mice on HFD have improved glucose metabolism. (**A**) Increased glucose and (**B**) insulin tolerance in female *Pomc-Cre Pparg*$^{fl/fl}$ animals (n = 5) compared with controls (n = 8). (**C** and **D**) Graphs shown a significant decrease in the liver gluconeogenesis of *Pomc-Cre Pparg*$^{fl/fl}$ mice compared with matched controls, as shown by the liver mRNA levels of (**C**) *Pepck* (n = 4 per group) and (**D**) *G6pase* (n = 4 per group). Data in all graphs are shown as mean ± SEM. *P < 0.05 compared with controls.

shown to induce different metabolic outcomes according to the timing of neuronal ablation (11, 20). Furthermore, recent data showed that multiple lineages of hypothalamic neurons express POMC during development, including a subpopulation of arcuate AgRP neurons that does not express POMC in adult mice (21). However, a very recent study using a new model of *POMC-Cre* mice showed that gene deletion in POMC neurons either prenatally or postnatally did not change the metabolic outcomes (21). Nevertheless, we cannot exclude the possibility that PPARγ deletion in a subpopulation of AgRP neurons may have contributed to the metabolic phenotype of our *Pomc-Cre Pparg*$^{fl/fl}$ mice, as changes in ROS levels in AgRP neurons have been shown to inactivate these neurons, thus reinforcing the anorexigenic tone of POMC neurons (7, 8).

In summary, our data showed that PPARγ deletion in POMC neurons dramatically affected cellular biological processes and activity of POMC neurons on HFD. These observations give further support to the notion that appropriate cellular biological adaptations in hypothalamic neurons, including ROS control, represent crucial components in leptin sensitivity and resistance and related metabolic and glucose control.

Methods

Mice and diet. All animal procedures described below have been approved by the Yale University Institutional Animal Care and Use Committee. Mice were kept under standard laboratory conditions, with free access to food and water. Mice were fed HFD for 16 weeks, starting at 8 weeks of age. All the experiments were performed at 12 weeks

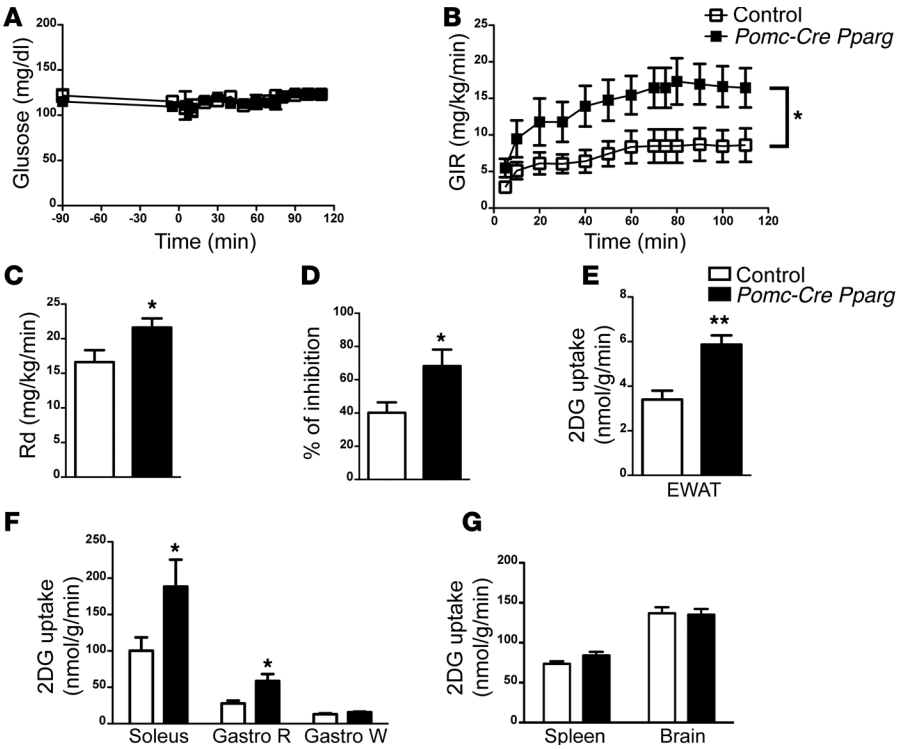

Figure 6. *Pomc-Cre Pparg*$^{fl/fl}$ mice on HFD have increased insulin sensitivity. (**A**) Glucose levels during the hyperinsulinemic-euglycemic clamp study in control (n = 7) and *Pomc-Cre Pparg*$^{fl/fl}$ mice (n = 6). (**B**) Graph showing a significant greater glucose infusion rate (GIR) during the hyperinsulemic-euglycemic clamp study in *Pomc-Cre Pparg*$^{fl/fl}$ mice compared with controls. (**C**) The increase in the rate of whole-body glucose disappearance (Rd) in *Pomc-Cre Pparg*$^{fl/fl}$ mice compared with controls. (**D**) Graph showing increased percentage of inhibition of hepatic glucose production in *Pomc-Cre Pparg*$^{fl/fl}$ mice compared with controls during the hyperinsulemic-euglycemic clamp study. (**E** and **F**) The increase in 2DG uptake in (**E**) EWAT and (**F**) muscles (soleus and Gastro-R) in *Pomc-Cre Pparg*$^{fl/fl}$ mice compared with controls. (**G**) No difference in 2DG uptake was observed in the spleens and in the brains of *Pomc-Cre Pparg*$^{fl/fl}$ and control mice. Data in all graphs are expressed as the mean ± SEM. *P < 0.05; **P < 0.01.

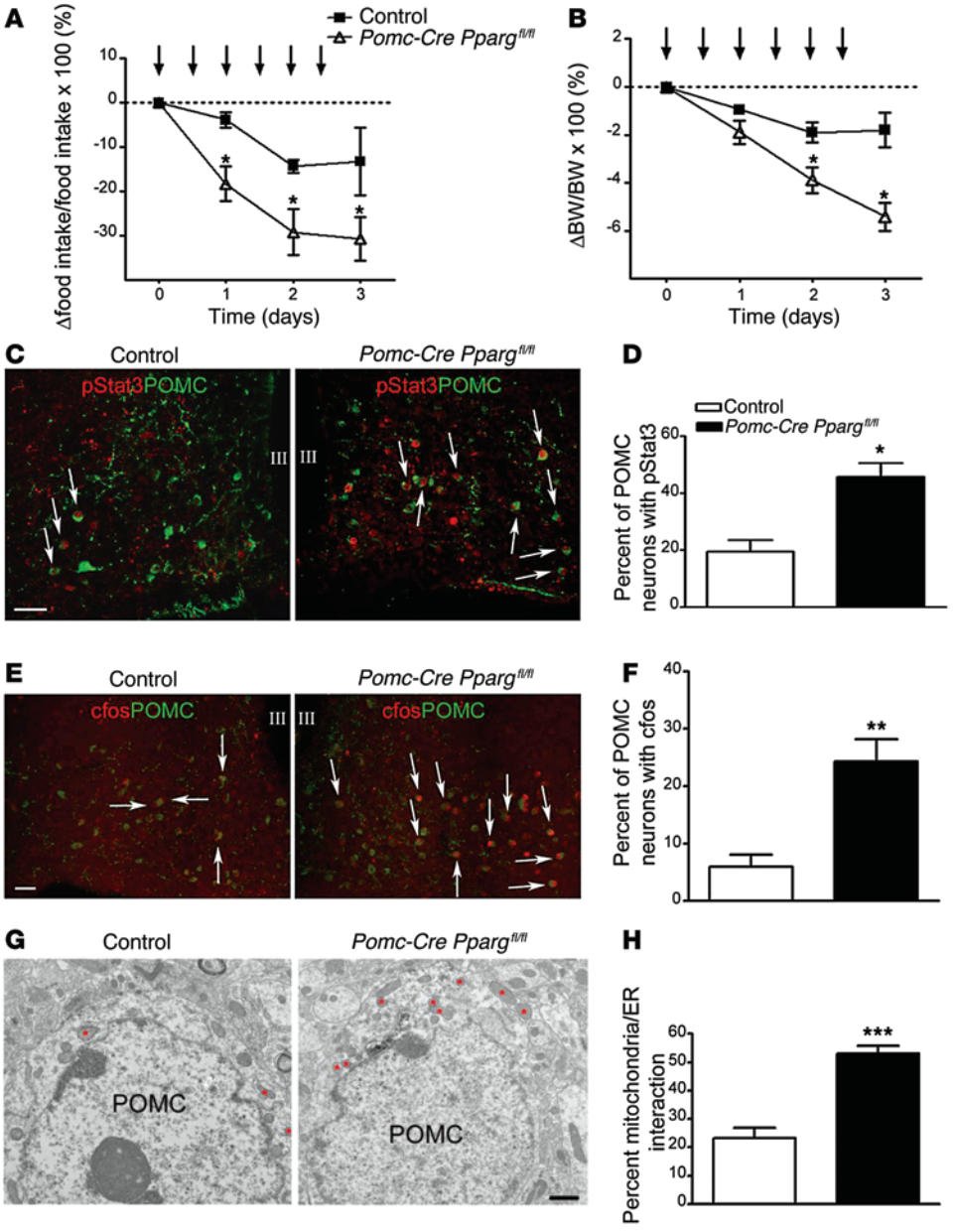

Figure 7. *Pomc-Cre Pparg*$^{fl/fl}$ mice on HFD are sensitive to leptin. (**A** and **B**) Daily food intake and body weight of control and *Pomc-Cre Pparg*$^{fl/fl}$ mice (n = 4–6 per group) treated with leptin for 3 days on HFD for 12 weeks. Arrows indicate leptin administration. (**C**) Representative confocal micrographs of p-STAT3 (red) and POMC (green) double immunolabeled hypothalamic sections (white arrows) from leptin-treated control and *Pomc-Cre Pparg*$^{fl/fl}$ mice. Scale bar: 50 μm. (**D**) A higher percentage of POMC neurons with p-STAT3–labeled nuclei in the arcuate nuclei of *Pomc-Cre Pparg*$^{fl/fl}$ mice was detected compared with controls (n = 4–6 per group). (**E**) Representative confocal photomicrographs of control and *Pomc-Cre Pparg*$^{fl/fl}$ mice double immunostained (white arrows) for POMC (green) and c-fos (red). Scale bar: 50 μm. (**F**) *Pomc-Cre Pparg*$^{fl/fl}$ mice showed an increased level of c-fos/POMC immunostaining in the arcuate nucleus of the hypothalamus compared with controls (n = 4–6 per group). (**G**) Electron micrographs showing representative sections of POMC perikarya in the arcuate nuclei from control and *Pomc-Cre Pparg*$^{fl/fl}$ mice. Red asterisks show mitochondria in close association with ER. Scale bar: 1 μm. (**H**) Quantification of mitochondria-ER interaction revealed higher numbers of mitochondria-ER contacts in POMC neurons of *Pomc-Cre Pparg*$^{fl/fl}$ animals compared with control animals (n = 4 per group). Data in all graphs are expressed as the mean ± SEM. *P < 0.05; **P < 0.01; ***P < 0.001.

of HFD unless otherwise reported. Daily food intake was assessed in individually housed mice. Regular diet was Purina Lab Chow 5001 (Ralston Purina), and HFD was Rodent Chow D12451 (Research Diets). All experiments described below were conducted on either *Pomc-Cre Pparg*$^{fl/fl}$ or *Pparg*$^{fl/fl}$-*Cre* negative male and female mice. *Pparg*$^{fl/fl}$ (B6.129-*Ppargtm2Rev*/J) and *Pomc-Cre* [Tg(-Pomc1-Cre)16Lowl/J] mice were purchased from The Jackson Laboratory and bred at Yale University. These 2 colonies were crossed to generate offspring heterozygous for the floxed PPARγ allele, which were *Pomc-Cre* transgene positive (*Pomc-Cre Pparg*$^{fl/+}$ mice). These mice were further mated with mice homozygous for the floxed PPARγ allele. The littermates of these breeders, mice homozygous for the floxed PPARγ with no Cre expression (*Pparg*$^{fl/fl}$ mice; controls) and mice homozygous for the floxed PPARγ with Cre expression (*Pomc-Cre Pparg*$^{fl/fl}$ mice; experimental knockout mice), were used in this study. In addition, *Pomc-Cre Pparg*$^{fl/+}$ mice were also used to test the effect of the *Cre* transgene on the metabolic phenotype.

In situ hybridization. To detect gene expression of *Pparg* in POMC neurons in the hypothalamus, we performed double hybridization, combining in situ hybridization and immunohistochemistry. To this end, we designed a riboprobe specific to mouse *Pparg* mRNA (NM_011146). First, we performed an in situ hybridization for PPARγ following a protocol previously reported (22, 23). Briefly, digoxigenin-labeled riboprobes were applied onto the slides with brain sections, with medial basal hypothalamic area at 20-μm thickness, and hybridized overnight at 50°C. The following day, the sections went through regular washing steps as reported previously (22, 23). The sections were then incubated with TNB blocking buffer for 30 minutes at room temperature (RT) and antibody (anti-DIG-POD antibody from Roche Diagnostic; 1:1,000 dilution in TNB buffer) for 2 hours at RT. To visualize the signal, the sections were incubated with tyramide system (Alexa Fluor 594 TSA Kit from Invitrogen) for 30 minutes at RT. Regular TNT washing was performed between

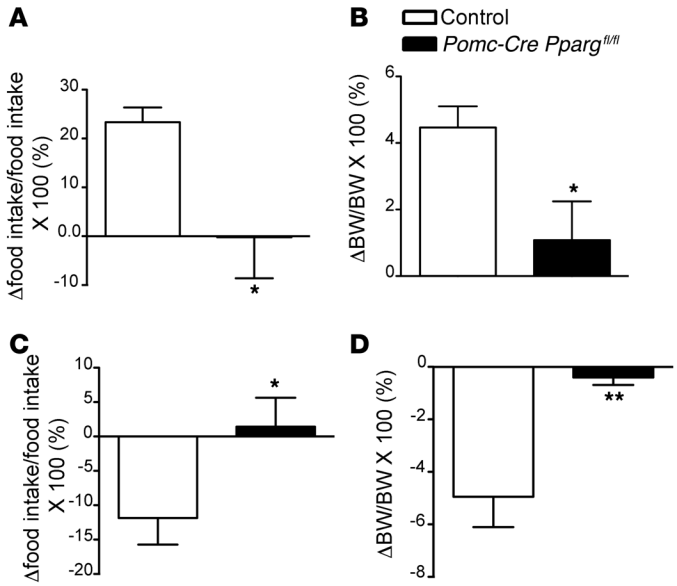

Figure 8. Peripheral administration of either rosiglitazone or GW9662 fails to affect food intake in *Pomc-Cre Pparg*$^{fl/fl}$ mice. (**A**) The effect of rosiglitazone administration on the food intake of lean control mice exposed to HFD (n = 5–6 per group). The percentage change in food intake before (vehicle treated) and after rosiglitazone treatment shows that rosiglitazone did not significantly alter food intake in *Pomc-Cre Pparg*$^{fl/fl}$ mice. (**B**) The effect of rosiglitazone administration on the body weight of lean control mice exposed to HFD. The percentage change in body weight before (vehicle treated) and after rosiglitazone treatment shows that rosiglitazone did not significantly alter body weight in *Pomc-Cre Pparg*$^{fl/fl}$ mice. (**C**) The effect of GW9662 administration on HFD-exposed mice for 16 weeks (n = 6 per group). The percentage change in food intake before (vehicle treated) and after GW9662 treatment shows that GW9662 failed to significantly decrease food intake in *Pomc-Cre Pparg*$^{fl/fl}$ mice. (**D**) The effect of GW9662 administration on the body weight of HFD-exposed mice for 16 weeks. The percentage change in body weight before (vehicle treated) and after GW9662 treatment shows that GW9662 failed to significantly decrease body weight in *Pomc-Cre Pparg*$^{fl/fl}$ mice. Data in the graphs are expressed as the mean ± SEM. *P < 0.05; **P < 0.01.

each antibody incubation step. Next, 0.3% H_2O_2 was applied onto the sections for 30 minutes at RT and washed out through regular 0.1 M PB buffer. The sections were incubated with milk blocking buffer (3% fat-free milk, 0.3% Triton X-100 in 0.1 M PB) for 30 minutes at RT, and then a series of antibody incubations was performed as follows: primary anti-POMC antibody from Phoenix Pharm., 1:1,000 dilution in 0.1 M PB for 2 hours, and Alexa Fluor 488–conjugated secondary donkey anti-rabbit IgG from Life Tech., 1:500 dilution in 0.1 M PB. Regular washing steps using 0.1 M PB were conducted between each antibody incubation step. Finally, the sections were cover slipped and subjected to microscopy.

Measurement of EE and body composition. Male and female *Pomc-Cre Pparg*$^{fl/fl}$ and control mice (on either standard chow diet or HFD) were individually housed 1 week before the measurements at RT (22°C) under an alternating 12-hour-light/12-hour-dark cycle. Animals were then transferred in metabolic cages (TSE PhenoMaster System Inc.). Parameters were automatically measured every 30 minutes for 1 week. Locomotor activity was determined for 5 days using a multidimensional infrared light beam system, with beams installed on cage bottom and cage top levels. Simultaneously, O_2 consumption, CO_2 production, and heat production were measured to determine the EE. EE was analyzed either after normalization by lean mass or using the ANCOVA analysis. In addition, food intake was determined continuously by integration of weighing sensors fixed at the top of the cage, from which the food containers have been suspended into the sealed cage environment. Body composition was measured in vivo by magnetic resonance imaging (EchoMRI; Echo Medical Systems).

Serum measurements. Serum from each blood sample was obtained by centrifugation at 1,500 *g* for 15 minutes. Serum levels of leptin, insulin, thyroid hormones (free T4 and T3), and corticosterone were measured by ELISA using commercially available kits (Millipore for leptin and insulin; Leinco Technologies for Free T4 and Free T3; Abnova Corporation for corticosterone).

Surgical procedures. For the hyperinsulinemic-euglycemic clamp, polyethylene catheters were inserted into the right carotid arteries and jugular veins of mice after they were anesthetized with ketamine (100 mg/kg body mass) and xylazine (10 mg/kg). Animals were individually housed after surgery, and lines were flushed daily with 50 μl heparinized saline for the 3-day recovery period.

Hyperinsulinemic-euglycemic clamp and measurement of 2DG uptake. The hyperinsulinemic-euglycemic clamp was measured as described previously (24, 25) and initiated in conscious and unrestrained mice after fasting for 4 hours. The 90-minute basal period (t = –90 to 0 minutes) was followed by a 115-minute clamp period (t = 0 to 115 minutes). A priming dose of [3-^{3}H]glucose (5 μCi) (Perkin Elmer) was administered at t = –90 minutes and was followed by infusion of the tracer at a rate of 0.05 μCi/min for 1.5 hours. For assessment of rate of appearance during the basal period, blood samples (50 μl) were collected at t = –15 and –5 minutes.

The clamp period was initiated at t = 0 minutes by primed and continuous infusion of human insulin (bolus of 16 mU/kg followed by a rate of 2.5 mU kg^{-1} min^{-1}) (Humulin R; Eli Lilly). The rate of [3-^{3}H] glucose infusion was increased to 0.1 μCi/min for the remainder of the experiment in order to minimize changes in specific activity relative to the equilibration period. Blood was collected every 5 to 10 minutes from the carotid artery catheter, and blood glucose was monitored (One Touch Ultra; LifeScan, Johnson & Johnson). Glucose (30%) was infused at a variable rate via the jugular vein catheter in order to maintain blood glucose levels at 110 to 130 mg/dl. Withdrawn erythrocytes were suspended in sterile 0.9% saline and returned to each animal.

Tissue 2DG uptake was measured as described previously (24). For assessment of 2DG uptake, mice were infused with 2DG (10 μCi) at t = 70 minutes, and blood samples (50 μl) were collected at t = 75, 85, 95, 105, and 115 minutes. Immediately after collection of the final blood sample (t = 115 minutes), mice were euthanized, and soleus, Gastro-R, white portion of gastrocnemius (Gastro-W), interscapular BAT, heart, spleen, EWAT, brain (cortex), and the liver were rapidly dissected. Gastro-R was dissected from the inner surface of gastrocnemius, which attaches to soleus muscle, while Gastro-W was dissected from the outer surface of the muscle. Rd, which reflects whole-body glucose utilization, and endogenous glucose production were determined as described previously (25).

Dihydroethidium. ROS levels in POMC neurons were measured as previously described (8). Briefly, in vivo ROS levels in POMC neurons

were measured by injecting dihydroethidium (DHE), as it is specifically oxidized by superoxide to red fluorescent ethidium. A 1 mg/ml concentration was injected into the tail veins of female *Pomc-Cre Pparg$^{fl/fl}$* and control mice either on standard chow diet or HFD. Mice were then transcardially perfused 3 hours later with 0.9% saline plus heparin followed by fixative (4% paraformaldehyde, 15% picric acid, 0.1% glutaraldehyde in 0.1 M phosphate buffer [PB]). Brains were collected and postfixed overnight before 50-μm coronal sections were cut. Immunocytochemistry for POMC was performed using a rabbit anti-POMC antisera (diluted 1: 1,000 in 0.1 M PB; Phoenix Pharmaceuticals). After overnight incubation in the primary antibody, sections were washed and incubated with fluorescent secondary antibodies (donkey anti-rabbit Alexa Fluor 488 diluted 1:500 in 0.1 M PB for 2 hours at RT; Invitrogen). Sections were then washed and mounted with VectaShield antifade (Vector Laboratories) for imaging of immunostained sections with a confocal microscope (Olympus). Fluorescent intensity was measured by ImageJ (NIH) to calculate fluorescence density per μm^2 POMC cytosol. 10 to 15 cells were analyzed per each mouse.

Mitochondria and peroxisomes counts and mitochondria-ER interaction analysis. Female *Pomc-Cre Pparg$^{fl/fl}$* and control mice exposed to HFD for 12 weeks were transcardially perfused as described above, and their brains were processed for electron microscopic examination as previously described (8). Briefly, POMC immunolabeling was performed overnight using a rabbit anti-POMC antisera (diluted 1:2,000 in 0.1 PB), followed by a secondary biotinylated anti-rabbit IgG diluted 1:500 in 0.1 M PB for 2 hours and ABC Elite (diluted 1:200 in 0.1 M PB; Vector Laboratories) for 2 hours. Visualization of POMC neurons was performed with diaminobenzidine. Sections were then processed for electron microscopic examination. Ultrathin sections were cut on a Leica ultramicrotome, collected on Formvar-coated single-slot grids, and analyzed with a Tecnai 12 Biotwin (FEI) electron microscope. Mitochondria and peroxisomes were counted blindly from randomly selected sections, and Scion Image was used to normalize cytoplasmic area so that mitochondrial number per cell was expressed in square micrometers as previously described (7). The same images were used for mitochondria-ER interaction analyzes. The number of mitochondria in juxtaposition to ER were counted and divided by the total number of mitochondria in the same cell to generate an index of mitochondria-ER interaction (11). All investigators were blinded to the experimental groups during the entire procedure.

Real-time PCR. RNAs from liver, BAT, and pituitary were extracted from male *Pomc-Cre Pparg$^{fl/fl}$* and control mice for *Pepck* and *G6pase* gene expression in the liver, *Ucp1* gene expression in the BAT, and *Pomc* gene expression in the pituitary. Total RNA (0.5–1 μg) was reverse transcribed using a High Capacity cDNA RT Kit (Applied Biosystems). Real-time PCR with diluted cDNA was performed using the LightCycler 480 (Roche) and TaqMan Gene Expression Assay primers (catalog no. Mm 00839363_m1 for *Pepck*; Mm 01247059_g1for *G6pase*; Mm 00435874_m1 for *Pomc*; Applied Biosystems) in a 20 μl reaction volume in duplicates. The calculations of average crossing point values, SD, and resulting expression ratios for each target gene were performed using Roche LightCycler 480 software.

Leptin sensitivity. Female *Pomc-Cre Pparg$^{fl/fl}$* and control mice on HFD were individually housed, and sham (vehicle) was injected for 5 days prior to leptin treatment. Recombinant murine leptin (1.5 μg/g body weight, Peprotech) was injected i.p. twice daily (at 8:00 and 19:00) for 3 days. Body weight and food intake were measured daily at 8:00. One hour after the last injection on day 3, mice were rapidly perfused, and brains were processed for double staining for either p-STAT3 and POMC or c-fos and POMC. p-STAT3 (Tyr705), c-fos, and POMC immunofluorescent stainings were carried out as described above (7). For p-STAT3 staining, antigen retrieval was performed by boiling the sections in citrate buffer (pH 8.5) preheated to 80°C in water. After washing and blocking with 2% normal horse serum, sections were incubated with primary antibodies. Rabbit antisera against p-STAT3, (1:250 in 0.1 M PB; Cell Signaling Technology) and c-fos (diluted 1:2,500 in 0.1 M PB; Calbiochem) were analyzed in different sets of sections at 4°C overnight. The following day, sections were washed and incubated with fluorescent secondary antibodies (donkey anti-rabbit Alexa Fluor 594 diluted 1:500 in 0.1 M PB for 2 hours at RT). Sections were then washed and immunostained for POMC (1:1,000 at 4°C overnight). The following day, after an incubation with fluorescent secondary antibodies (donkey anti-rabbit Alexa Fluor 488 diluted 1:500 for 2 hours at RT), sections were washed and mounted with VectaShield antifade (Vector Laboratories) for analysis.

Peripheral injection of rosiglitazone and GW9662. PPARγ agonist rosiglitazone (Cayman Chemicals) was dissolved in 10% DMSO. Sixteen-week-old female *Pomc-Cre Pparg$^{fl/fl}$* and control mice (n = 5–6) on regular chow diet were switched to HFD and injected with vehicle for 5 days. After 5 days, rosiglitazone was injected i.p. for 5 consecutive days at a dose of 28 mg/kg body weight. Food intake was measured daily. Body weight was measured at the start and the end of the treatment.

PPARγ antagonist GW9662 (Cayman Chemicals) was dissolved in 25% DMSO. Male *Pomc-Cre Pparg$^{fl/fl}$* and control mice exposed to HFD for 16 weeks (n = 6) were injected first for 5 days i.p. with vehicle and then with GW9662 at a dose of 2 mg/kg body weight for 5 consecutive days. Food intake was measured daily. Body weight was measured at the start and the end of the treatment.

For both rosiglitazone and GW9662, food was removed from the cages 6 hours before the onset of the dark cycle. Both rosiglitazone and GW9662 were administered 3 hours before the onset of the dark cycle. Daily food intake was recorded at 8:00 in the light cycle.

Statistics. All data are expressed as the mean ± SEM. The means between 2 groups were analyzed by 2-tailed Student's t test, and the means among more than 2 groups and 2 genotypes were analyzed by 2-way analysis of variance, followed by Bonferroni post-hoc tests, unless otherwise stated. ANCOVA was used to analyze the effect of both genotype and body weight on EE, VO_2, and VCO_2. Significance was taken at $P < 0.05$.

Study approval. All animal procedures described have been approved by the Yale University Institutional Animal Care and Use Committee.

Acknowledgments

This work was supported by NIH grant DK 097566 (to S. Diano).

Address correspondence to: Sabrina Diano, Department of Obstetrics, Gynecology, and Reproductive Sciences, Yale University School of Medicine, PO Box 208063, New Haven, Connecticut 06520-208063, USA. Phone: 203.737.1216; E-mail: sabrina.diano@yale.edu.

1. Lehrke M, Lazar MA. The many faces of PPARγ. *Cell*. 2005;123(6):993–999.
2. Shimizu H, Tsuchiya T, Sato N, Shimomura Y, Kobayashi I, Mori M. Troglitazone reduces plasma leptin concentration but increases hunger in NIDDM patients. *Diabetes Care*. 1998;21(9):1470–1474.
3. Larsen PJ, et al. Differential influences of peroxisome proliferator-activated receptors γ and -α on food intake and energy homeostasis. *Diabetes*. 2003;52(9):2249–2259.
4. Sarruf DA, et al. Expression of peroxisome proliferator-activated receptor-gamma in key neuronal subsets regulating glucose metabolism and energy homeostasis. *Endocrinology*. 2009;150(2):707–712.
5. Ryan KK, Li B, Grayson BE, Matter EK, Woods SC, Seeley RJ. A role for central nervous system PPAR-γ in the regulation of energy balance. *Nat Med*. 2011;17(5):623–626.
6. Lu M, et al. Brain PPAR-γ promotes obesity and is required for the insulin-sensitizing effect of thiazolidinediones. *Nat Med*. 2011;17(5):618–622.
7. Diano S, et al. Peroxisome proliferation-associated control of reactive oxygen species sets melanocortin tone and feeding in diet-induced obesity. *Nat Med*. 2011;17(9):1121–1127.
8. Andrews ZB, et al. UCP2 mediates ghrelin's action on NPY/AgRP neurons by lowering free radicals. *Nature*. 2008;454(7206):846–851.
9. Zhang X, Zhang G, Zhang H, Karin M, Bai H, Cai D. Hypothalamic IKKβ/NF-κB and ER stress link overnutrition to energy imbalance and obesity. *Cell*. 2008;135(1):61–73.
10. Ozcan L, et al. Endoplasmic reticulum stress plays a central role in development of leptin resistance. *Cell Metab*. 2009;9(1):35–51.
11. Schneeberger M, et al. Mitofusin 2 in POMC neurons connects ER stress with leptin resistance and energy imbalance. *Cell*. 2013;155(1):172–187.
12. Pinto S, et al. Rapid rewiring of arcuate nucleus feeding circuits by leptin. *Science*. 2004;304(5667):110–115.
13. Myers MG, Myers MG Jr, Leibel RL, Seeley RJ, Schwartz MW. Obesity and leptin resistance: distinguishing cause from effect. *Trends Endocrinol Metab*. 2010;21(11):643–651.
14. Munzberg H, Flier JS, Bjorbaek C. Region-specific leptin resistance within the hypothalamus of diet-induced obese mice. *Endocrinology*. 2004;145(11):4880–4889.
15. Mori H, et al. Socs3 deficiency in the brain elevates leptin sensitivity and confers resistance to diet-induced obesity. *Nat Med*. 2004;10(7):739–743.
16. Dreyer C, Krey H, Givel F, Helftenbein G, Wahli W. Control of the peroxisomal β-oxidation pathway by a novel family of nuclear hormone receptors. *Cell*. 1992;68(5):879–887.
17. I Green S. Activation of a member of the steroid hormone receptor superfamily by peroxisome proliferators. *Nature*. 1990;347(6294):645–650.
18. del Rio LA, Sandalio LM, Palma JM, Bueno P, Corpas FJ. Metabolism of oxygen radicals in peroxisomes and cellular implications. *Free Radic Biol Med*. 1992;13(5):557–580.
19. Dietrich MO, Liu ZW, Horvath TL. Mitochondrial dynamics controlled by mitofusins regulate agrp neuronal activity and diet-induced obesity. *Cell*. 2013;155(1):188–199.
20. Gropp E, et al. Agouti-related peptide-expressing neurons are mandatory for feeding. *Nat Neurosci*. 2005;8(10):1289–1291.
21. Padilla SL, Carmody JS, Zeltser LM. Pomc-expressing progenitors give rise to antagonistic neuronal populations in hypothalamic feeding circuits. *Nat Med*. 2010;16(4):403–405.
22. Kwon Jeong J, Dae Kim J, Diano S. Ghrelin regulates hypothalamic prolyl carboxypeptidase expression in mice. *Mol Metab*. 2013;2(1):23–30.
23. Jeong JK, Szabo G, Kelly K, Diano S. Prolyl carboxypeptidase regulates energy expenditure and the thyroid axis. *Endocrinology*. 2012;153(2):683–689.
24. Toda C, et al. Extracellular signal-regulated kinase in the ventromedial hypothalamus mediates leptin-induced glucose uptake in red-type skeletal muscle. *Diabetes*. 2013;62(7):2295–2307.
25. Ayala JE, Bracy DP, McGuinness OP, Wasserman DH. Considerations in the design of hyperinsulinemic-euglycemic clamps in the conscious mouse. *Diabetes*. 2006;55(2):390–397.